PAPER

Check for updates

Dynamic regulation of ion transport through a bis(1,3-propanediol)-based channel *via* allosteric azobenzene photoswitching†

Manzoor Ahmad, [ID] ‡[a] Susmita Sarkar,[b] Ravindra Bhogade,[a] Abhishek Mondal, [ID] [a,c] Debashis Mondal, [ID] §[a] Jagannath Mondal [ID] [b] and Pinaki Talukdar [ID] *[a]

The transportation of ions across cell membranes is vital in biological functions and is frequently controlled by external triggers like light, ligands, and voltage. Synthetic ion transport systems, particularly those featuring gating mechanisms, have attracted considerable interest. In this research, we engineered self-assembled barrel rosette ion channels using a photoresponsive azobenzene integrated at an allosteric site. Morphological studies verified more effective self-assembly of the *trans* form in contrast to the *cis* form. The restricted self-assembly of the *cis* form can be ascribed to the nonplanar structure of *cis* azobenzene moieties, which inhibits favorable π–π stacking interactions. The ion transport studies demonstrated the formation of ion channels by the *trans* form with anion antiport as the primary transport mechanism. In contrast, the *cis* form exhibited lower efficiency. Based on these observations, dynamically gated ion transport was achieved by employing two sets of electromagnetic radiation at 365 nm and 450 nm, respectively. Molecular dynamics simulation studies demonstrated that the channel formed by assembling *trans* monomers exhibited greater stability when compared to the channel formed by *cis* monomers. Additionally, the *trans* channel was found to recognize and transport chloride effectively.

Introduction

Artificially designed synthetic ion transport systems have emerged as an important class of compounds that have shown potential applications as therapeutics for cancer treatment and diseases that occur due to the malfunctioning of naturally occurring ion channels like cystic fibrosis.[1–4] Although a wide variety of synthetic mimics in the form of ion channels[5–7] and ion carriers[8,9] have been developed, gated systems that promise better applications are very rare. Stimuli like light,[10] enzymes,[11] pH,[12] voltage,[13] ligands,[14] *etc*. are utilized to generate artificially gated ion transport systems. Light, because of its spatiotemporal control, remote addressability, tunable

intensity, and less toxicity, is considered to be more effective compared to other stimuli.[15] Different kinds of photosystems that have been employed include the use of photoswitches (*e.g.*, azobenzene, acylhydrazone, phenylhydrazone, stilbene, spiropyrans, *etc*.)[16–22] or photocleavable groups (*e.g.*, *o*-nitro aromatics, bodipy, *etc*.).[23,24] Azobenzene is one of the versatile photoswitches that is mostly used because of its spatial and temporal control, significant change in length and dipole moment upon *cis–trans* photoisomerization, and very quick response time of action.[25] Most of these systems developed are photoresponsive ion carriers due to the lack of sophisticated designs for the construction of ion channels. Self-assembly is one of the ways to construct artificial ion channels by employing different non-covalent interactions like hydrogen bonding, π–π interactions, halogen bonding interactions, *etc*.[26] Precisely, the incorporation of a photoswitch like azobenzene,[27] acylhydrazone,[28] *etc*. into these motifs can provide an opportunity to externally control the self-assembly pattern and thereby control the ion transport activity across the lipid bilayer membrane. In this context, Linyong Zhu and colleagues employed an azobenzene subunit linked to crown ether groups to create cation channels arranged in parallel stacks within the lipid bilayer membrane, demonstrating photoresponsive characteristics.[29] However, the construction of self-assembled photoresponsive anion channels poses a challenge due to the necessity for intricate design strategies and the absence of sophisti-

[a]*Department of Chemistry, Indian Institute of Science Education and Research Pune, Dr Homi Bhabha Road, Pashan, Pune 411008, Maharashtra, India. E-mail: ptalukdar@iiserpune.ac.in*

[b]*Center for Interdisciplinary Sciences, Tata Institute of Fundamental Research, Hyderabad 500046, Telangana, India*

[c]*Leiden Institute of Chemistry, Leiden University, Einsteinweg 55, 2333 CC Leiden, The Netherlands*

†Electronic supplementary information (ESI) available. See DOI: https://doi.org/10.1039/d4nr01711k

‡Present Address: Chemistry Research Laboratory, Mansfield Road, Oxford, OX1 3TA, UK

§Present Address: Faculty of Chemistry, Biological and Chemical Research Centre, University of Warsaw, Zwirkii Wigury 101, Warsaw 02-089, Poland

cated functional units capable of forming anion channel structures within the lipid bilayer membrane.

Our laboratory has recently revealed self-assembled ion channels originating from bis(1,3-diol) connected to a 1,3-diethynylbenzene core.[30] These channels demonstrate noteworthy anion transport activity across the lipid bilayer membrane. The system employed intra- and inter-molecular hydrogen bonding interactions of 1,3-dihydroxyl moieties and π–π stacking interactions of 1,3-diethynylbenzene in stabilizing the ion channel. We predicted that customizing the core to include a photoswitch, specifically in the form of azobenzene, would offer light-responsive control over ion transport activity. Furthermore, introducing the azobenzene moiety at an allosteric site rather than within the channel cavity would not impede the ion transport process. The planarity of the *trans* form of 1,3-diethynylazobenzene was anticipated to enhance self-assembly, forming a stable ion channel through strong π–π stacking interactions among the azobenzene units. The assembly of such a channel could be disrupted upon exposure to 365 nm photoirradiation, primarily due to the photoisomerization of the planar *trans*-azobenzene to the nonplanar *cis*-azobenzene form (Fig. 1). The active form would further be reverted back upon photoirradiation at a different wavelength of light (450 nm). The incorporation of aliphatic chains into the azobenzene subunit was expected to provide lipophilic control and further strengthen the self-assembly behavior because of hydrophobic interactions.

Results and discussion

Synthesis

In order to synthesize the desired compounds **1a–1d**, initially, 3,5-diiodoaniline **2** was coupled with nitrosobenzene **3** in the
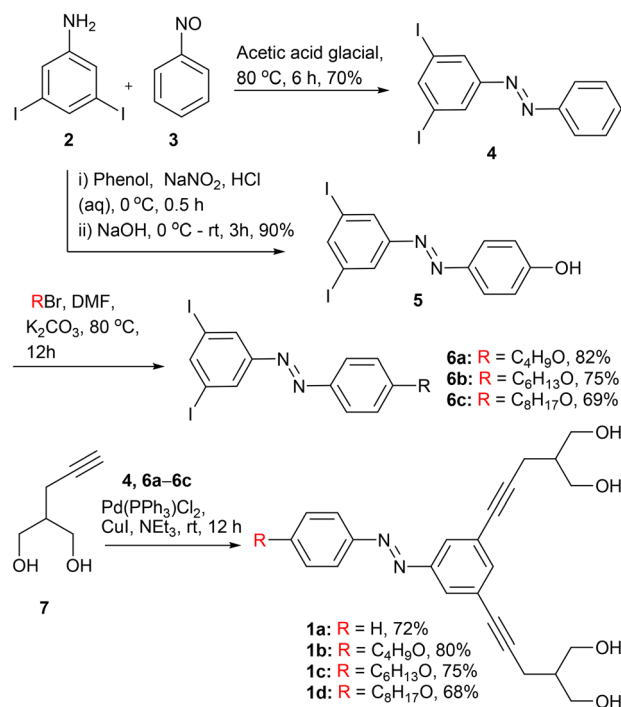
Scheme 1 Chemical synthesis of channel forming molecules **1a–1d**.

presence of glacial acetic acid to form diiodo azobenzene derivative **4** (Scheme 1). On the other hand, the diazotization reaction of **2** with phenol furnishes hydroxyl azobenzene **5** that, upon further reaction with different alkyl bromide compounds, furnishes azobenzene derivatives **6a–6c**. Finally, diiodo compounds **4** and **6a–6c** are coupled with 2-(prop-2-yn-1-yl) propane-1,3-diol **7** through the Sonagashira coupling reaction in the presence of Pd(PPh$_3$)$_4$ to furnish the desired final compounds **1a–1d** in 68–80% yields. All the compounds were fully characterized by ^{1}H NMR, ^{13}C NMR, IR, and HRMS techniques (Fig. S25–S46†).

Ion transport studies

After the synthesis of the desired compounds, the ion transport activity was evaluated. Initially, large unilamellar vesicles (LUVs) from egg-yolk phosphatidylcholine (EYPC) lipid entrapping 8-hydroxypyrene-1,3,6-trisulfonic acid trisodium salt (HPTS), 1 mM HPTS dye, and 100 mM NaCl were prepared and buffered at pH 7.0 using 10 mM HEPES buffer.[31] The ion transport activity was monitored by recording the change in the fluorescence intensity of the HPTS dye λ_{em} = 510 nm (λ_{ex} = 450 nm) occurring due to the disruption of the pH gradient created by adding an aqueous solution of sodium hydroxide in the external buffer. The ion transport activity sequence recorded at 10 μM concentration was found to be **1d** > **1c** > **1b** > **1a** (Fig. 2A). The above sequence suggests that long chain alkyl groups because of their higher lipophilicity would most likely result in better lipid permeation which eventually results in better ion transport activity. Dose-dependent studies furnished EC_{50} values of 1.74 μM and 2.39 μM for compounds **1d**
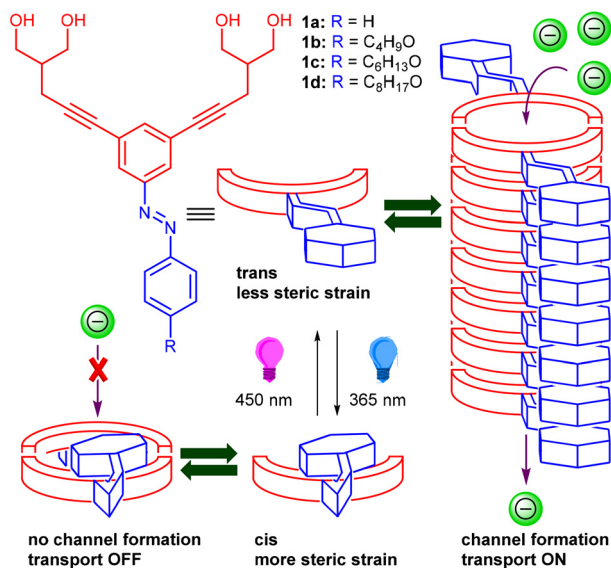
Fig. 1 Schematic representation of the structures of the designed molecules and photoresponsive ion transport through azobenzene-based ion channel structures.
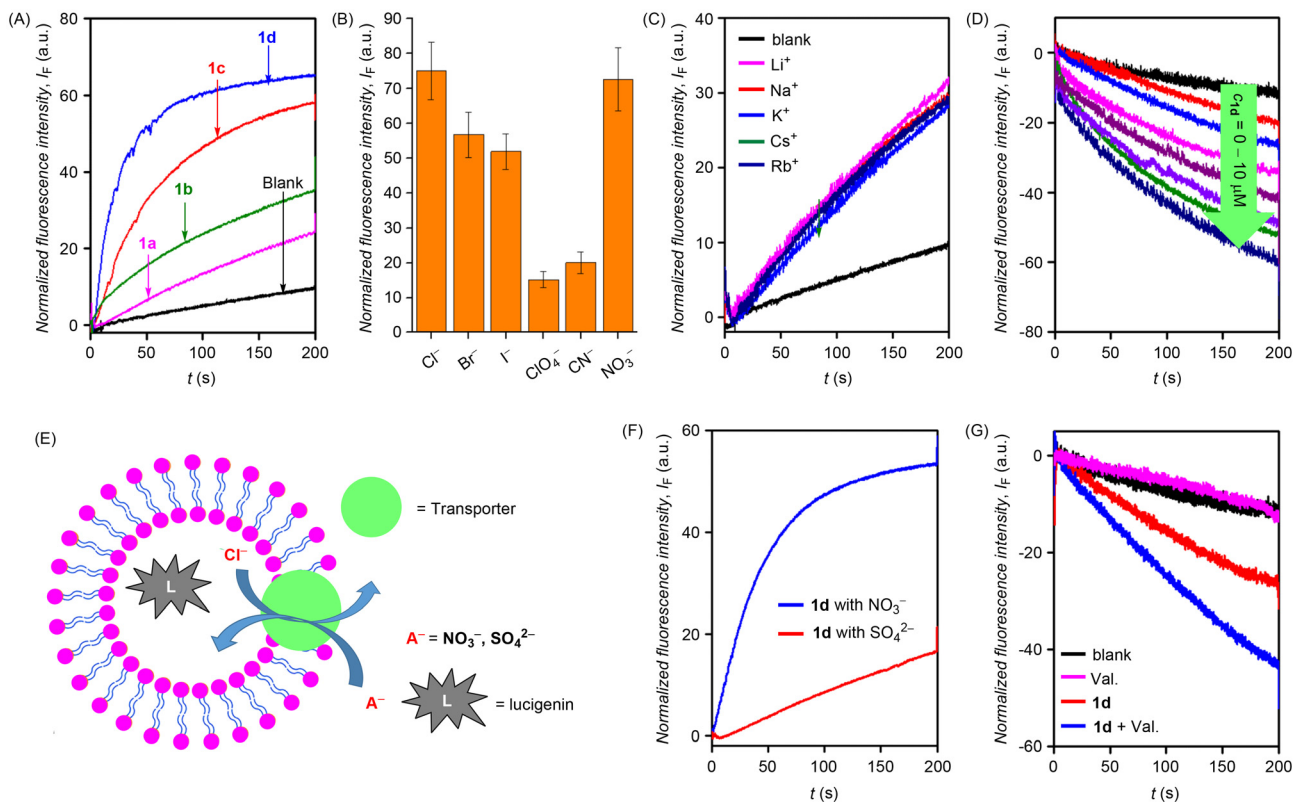
Fig. 2 Activity comparison of **1a**–**1d** across EYPC-LUVs ⊃ HPTS (10.0 μM) (A). Transport activity of **1d** (5.0 μM) by varying external anions across EYPC-LUVs ⊃ HPTS; each bar graph represents mean ion transport activity, calculated from three independent experiments (B). Transport activity of **1d** (0.3 μM) measured by varying external cations (M⁺ = Li⁺, Na⁺, K⁺, Rb⁺, Cs⁺) across EYPC-LUVs ⊃ HPTS (C). Concentration-dependent activity of compound **1d** across EYPC-LUVs ⊃ Lucigenin (D). Schematic representation of lucigenin-encapsulated antiport assay (E). Efflux of the Cl⁻ ion by **1d** (10.0 μM) in the presence of extravesicular SO_4^{2-} or extravesicular NO_3^{-} ions (F). Normalized Cl⁻ influx by **1d** in the presence and absence of valinomycin (G).

and **1c**, respectively. The Hill coefficient was found to be $n \approx 1$, indicating the formation of the stable ion channel structures. The EC_{50} values of compounds **1a** and **1b** could not be evaluated because of the precipitation issues at higher concentrations.

Mechanistically, the ion transport in the above HPTS-based studies could occur through (a) H⁺/X⁻ symport, (b) OH⁻/X⁻ antiport, (c) H⁺/M⁺ antiport, or (d) OH⁻/M⁺ symport modes. On varying the cations in the external buffer using different MCl salt solutions (M⁺ = Li⁺, Na⁺, K⁺, Rb⁺, and Cs⁺), no change in the ion transport activity was observed, indicating no role of cations in the transport process (Fig. 2C). However, upon varying anions in the external buffer, by using different NaX salt solutions (X⁻ = Cl⁻, Br⁻, ClO₄⁻, CN⁻, NO₃⁻ and I⁻), a significant change in the ion transport activity was observed with the activity sequence of Cl⁻ > NO₃⁻ > Br⁻ > I⁻ > CN⁻ > ClO₄⁻ (Fig. 2B and S5B†) indicating the active role of anions in the transport process. These studies ruled out H⁺/M⁺ antiport or OH⁻/M⁺ symport ion transport modes and indicate that the ion transport could potentially occur in either H⁺/X⁻ symport or OH⁻/X⁻ antiport mode.

Subsequently, chloride transport for the most active compound **1d** was monitored across EYPC-LUVs ⊃ Lucigenin.

Vesicles entrapping a lucigenin dye were prepared, and a Cl⁻/NO₃⁻ gradient was created across the lipid membrane.[32] The transport of chloride was monitored by recording the time-dependent fluorescence quenching of the lucigenin dye at λ_{em} = 535 nm (λ_{ex} = 455 nm). Significant fluorescence quenching was observed upon the addition of **1d** (Fig. 2D). Hill analysis could not be performed because of the precipitation issues at higher concentrations. Mechanistically, the ion transport in the lucigenin assay could occur through (a) H⁺/Cl⁻ symport or (b) Cl⁻/NO₃⁻ antiport mode, as the other modes involving the role of cations have been ruled out in the HPTS studies. A modified lucigenin assay was performed to obtain further insights into the mechanism of ion transport. The chloride influx across the lipid vesicles containing intravesicular $NaNO_3$ (200 mM) and extravesicular KCl (200 mM) was monitored in the presence and absence of valinomycin (a highly selective K⁺ transporter).[33] A manifold enhancement in the ion transport activity suggests the cooperative effect of valinomycin and **1d** and thus indicates the Cl⁻/NO₃⁻ antiport mode as the primary mode of ion transport (Fig. 2G). No such cooperativity would have been possible in the case of H⁺/Cl⁻ symport mode. The antiport mechanism was further validated by performing the modified lucigenin assay. A lucigenin dye was encapsulated

within the liposomes containing NaCl (200 mM) buffered at a pH of 7.0. The effect of ion transport activity was monitored by the addition of either NaNO$_3$ (200 mM) or Na$_2$SO$_4$ (200 mM) in the external buffer. Significant transport activity was observed in the presence of NaNO$_3$, and no significant activity was observed in the presence of Na$_2$SO$_4$ (Fig. 2F). The above results suggest Cl$^-$/NO$_3^-$ antiport mode of ion transport rather than H$^+$/Cl$^-$ symport because, in the case of H$^+$/Cl$^-$ symport, no change should have occurred by changing the external buffer to either NaNO$_3$ or Na$_2$SO$_4$. In the case of the antiport mechanism, SO$_4^{2-}$ being very hydrophilic and highly hydrated is not transported easily.

Planar bilayer conductance studies

In order to confirm the formation of an active ion channel across the lipid bilayer, electrical conductance was measured for the most active compound **1d**.[34,35] For that, a lipid composed of 1,2-diphytanoyl-*sn*-glycerol-3-phosphocholine (DPhPC) was used, which separates the 1.0 M KCl solution-filled *cis* and *trans* chambers. The treatment of **1d** (2.0 μM) in the *trans* chamber, followed by the application of various holding potentials between the two compartments, produced significantly long single channel opening and closing events, demonstrating the development of stable ion channels by **1d** at the planar bilayer (Fig. 3A, B and S21†). The single-channel conductance value, calculated using Hille's equation including the Sansom correction factor 5.61,[36] was found to be 17.5 ± 0.8

pS, and the diameter of the channel was calculated to be 4.09 ± 0.19 Å. In the presence of the KCl symmetric solution (1.0 M each), current–voltage (*I*–*V*) graphs showed linear trends, indicating an ohmic characteristic for A (Fig. 3C). The non-dipolar structure of the channels accounts for this linearity. On the other hand, asymmetric KCl solutions were used to assess the ion selectivity of **1d** (0.5 M in the *trans* chamber and 1.0 M KCl in the *cis* chamber). The calculation of the permeability ratio revealed $P_{Cl-}/P_{K+} = 3.24$, confirming the anion-selective nature of **1d**.

Photoisomerization studies

The photoisomerization studies of compounds **1a**–**1d** were carried out through ^{1}H NMR spectroscopy and UV-Vis absorption studies. Initially, ^{1}H NMR spectra of the *trans* samples of **1a**–**1d** were recorded in DMSO-d_6. After that, each sample was photoirradiated at 365 nm for 20 min and NMR spectra were recorded again. The photoirradiation led to significant changes in the proton signals, indicating a *trans*-to-*cis* photoisomerization process with a *trans* : *cis* ratio of 08 : 92, 10 : 90, 12 : 88, and 11 : 89 for compounds **1a**, **1b**, **1c**, and **1d**, respectively at a photo-stationary state (PSS) (Fig. S14–S17†). UV-Vis absorption studies showed a distinct band at 355 nm corresponding to π–π* transition, which substantially decreased upon photoirradiation at 365 nm with the appearance of a new band at 450 nm corresponding to n–π* transition (Fig. S10A,
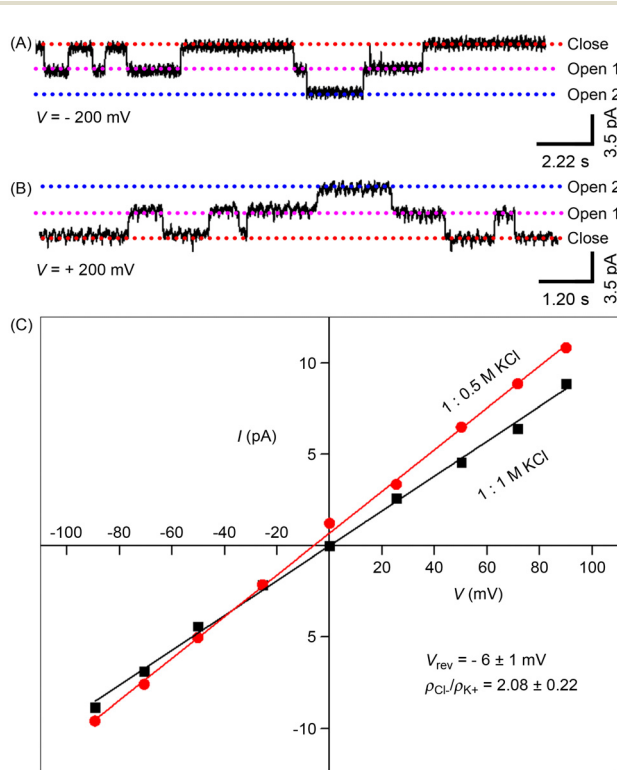

Fig. 3 Current traces recorded with **1d** (*c* = 2.0 μM) at −200 mV (A) and +200 mV (B) in a symmetrical KCl solution. Current–voltage relationship of **1d** in both symmetrical and asymmetrical KCl concentrations (C).
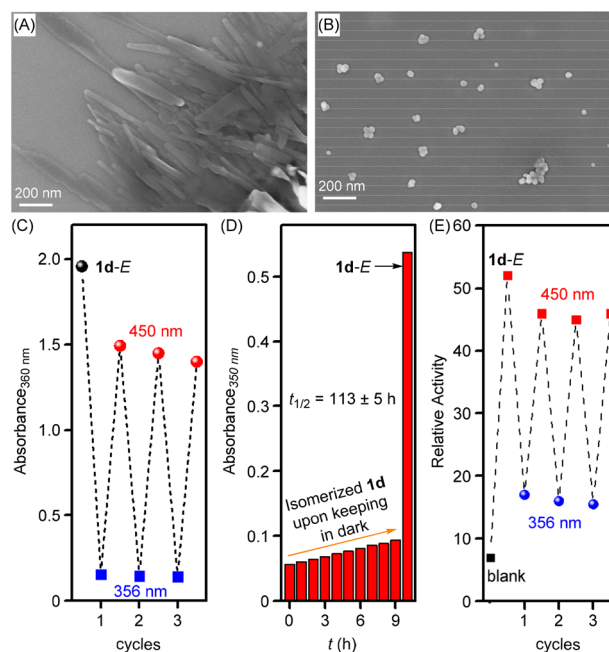

Fig. 4 FESEM images of **1d** in *trans* (A) and *cis* (B) forms showing distinct aggregation patterns recorded in methanol. Switching cycles for **1d** (20 μM) under alternating irradiation with 365 nm (10 s) and 450 nm (20 s) light, respectively (C). Change in absorption at 350 nm of **1d** (20 μM) upon keeping in the dark for 9 h (D). Photoregulated ion transport activity of **1d** (5.0 μM) taken at *t* = 280 s under alternating photoirradiation at two different wavelengths of 365 nm (15 s) and 450 nm (20 s) across EYPC-LUVs ⊃ HPTS (E).

S11A, S12A, and S13A†). These changes were consistent with the *trans*-to-*cis* photoisomerization process of the azobenzene subunit. The reverse *cis*-to-*trans* process was achieved by photoirradiating the *cis* compound at 450 nm of electromagnetic radiation (Fig. S10B, S11B, S12B, and S13B†). This reversible photoisomerization process was also achieved over three repeated cycles without any loss of efficiency (Fig. 4C, S10D, S11D, S12D and S13D†). Moreover, the *cis* form of **1d** showed excellent thermal stability while keeping in the dark for 9 h. The thermal relaxation from *cis*-to-*trans* follows a first-order rate law with a half-life period of 113 ± 5 h (Fig. 4D and S18†).

Furthermore, the solid-state morphological studies were performed using the field emission scanning electron microscopy (FESEM) technique in order to see the self-assembly behavior in the *trans* form and photoisomerized *cis* form of the channel-forming molecule **1d**. Initially, the sample of **1d** in methanol (100 μM) was prepared, dropcast on a silicon wafer, dried, and then used for morphology studies. The FESEM analysis shows rod-shaped structures in the *trans* form of **1d** in the solid state (Fig. 4A and S20A†). These rod-shaped structures are most likely the outcome of strong self-assembly assisted with strong π–π interactions of the azobenzene subunits and inter-molecular hydrogen bonding interactions of the bis(1,3-diol) moiety. However, when the *trans* sample of **1d**

in methanol was initially photoirradiated at 365 nm of light for 5 min and then used for the FESEM analysis, vesicular shaped structures were obtained (Fig. 4B and S20B†). This clearly indicates that the long-range self-assembled structures are getting disrupted in the *cis* form upon photoirradiation likely because of the formation of non-planar *cis* azobenzene with poor self-assembly as compared to the *trans* form.

After photoisomerization studies, photoresponsive ion transport studies were performed using HPTS-based vesicles. Compound **1d** showed efficient ion transport activity in the *trans* form at 0.25 μM concentration (used from 2 mM stock solution of **1d** in DMSO). However, upon photoirradiation at 365 nm using LEDs (3 × 1/3 watt) for 15 s, a significant decrease in the ion transport activity of **1d** was observed, likely due to the *trans* to *cis* photoisomerization process that disrupts the self-assembly and hence stops the ion channel formation (Fig. S19A†). On the other hand, when the photoisomerized solution (initially photoirradiated at 365 nm for 15 s) was photoirradiated at 450 nm of light using LEDs (3 × 1/3 watt) for 20 s, the ion transport activity was regained due to the *cis* to *trans* photoisomerization process (Fig. S19B†). This photoresponsive ion transport activity, regulated reversibly through alternating photoirradiation at 365 nm and 450 nm, was sustained over multiple cycles without any loss of efficiency (Fig. 4E).
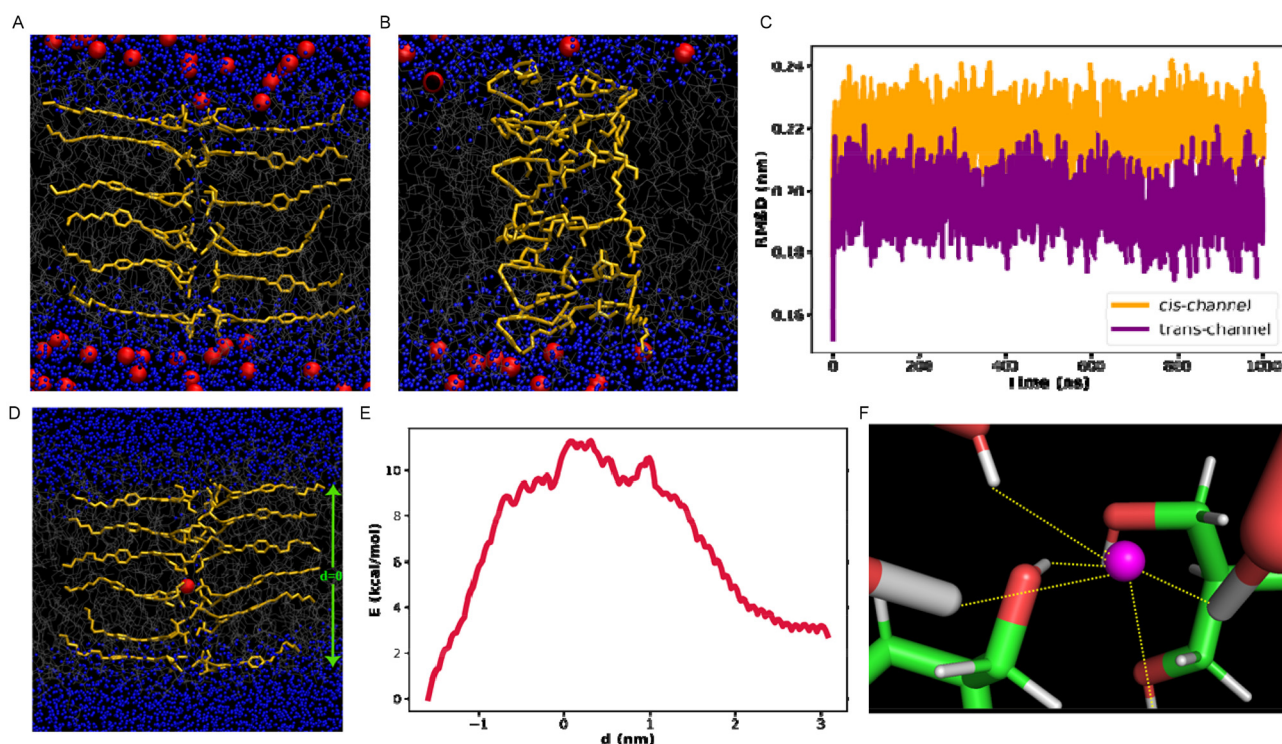

Fig. 5 Representative snapshots of self-assembled **1d**, *i.e.*, *trans* (A) and the corresponding *cis* (B) channel structures embedded within the lipid membrane during equilibrium simulation. Time profile of root mean square deviation (RMSD) of both the channels (*cis* and *trans*) during equilibrium simulation (C). Snapshot of *trans* channel displaying the collective variable, *d*, used in umbrella simulation (D) and free energy profile (calculated employing umbrella sampling simulation) of the Cl⁻ transport through the more stable *trans* channel represented corresponding to *cv* and *d* (E). The possible interactions between the Cl⁻ ion and the channel residues within the *trans* channel during ion progression (F).

Molecular modeling of the ion channel

To explore the underlying mechanism of ion passage through the channel and to assess the stability of the self-assembled channel on or before the ion transport, atomistic computer simulations were performed. Initially, we estimated the stability of each of the channel structures (*trans* and *cis*) and compared the time profile of root mean square deviation (RMSD) during equilibrium simulation for both channels. It was observed that the RMSD of the channel constituted with the *cis* monomers is higher compared to that of the *trans* channel and suggests that the *trans* channel structure remains relatively more stable compared to that of the *cis* structure (Fig. 5C). The snapshots in Fig. 5A and B also refer to the relatively more stable channel made up of the *trans* monomers than that of the *cis* form. We further proceeded to compute the free energy of the anion transport through the stable *trans* structure. From the free energy profile (Fig. 5E), it is evident that the free energy becomes maximum when the chloride ion remains in the middle of the channel, while the free energy decreases gradually when the anion moves towards either end of the channel structure, which is reflected by the fairly symmetric nature of the free energy profile on either side. The progress of the anion slows down in the center of the channel. Conversely, as the ion approaches the interface with bulk water, the free energy barrier considerably decreases due to its favorable interaction with an ample number of water molecules, which decreases toward the center (Fig. S22†). The presence of a sufficient amount of water within the channel core assists the ion in getting transported through the channel by maintaining a favorable solvent-rich environment, thereby not letting the free energy barrier increase to an unaffordable high limit. Furthermore, to gain mechanistic insights into chloride ion transport and to understand how the transport process is sensitive to the chemical nature of the channel, the interactions that are key for the ion movement through the channel structure were characterized. The contact of the chloride ion successively increases as the ion progresses through the channel, and it was observed that the favorable interactions with the channel monomers with the anion make the transport process easier (Fig. S23, S24† and Fig. 5F).

Conclusion

In conclusion, we developed azobenzene-fused bis(1,3-diol) molecules **1a–1d** for photo-responsive self-assembled ion channel formation utilizing intra- and inter-molecular hydrogen bonding interactions and π–π stacking interactions. Compound **1d**, with a long alkyl chain connected to the azobenzene subunit, furnished the highest ion transport activity with an EC_{50} value of 1.74 μM. The Hill coefficient value of ~1 indicates the formation of a stable ion channel structure inside the lipid bilayer membrane. The planar bilayer conductance measurement studies also supported the formation of stable ion channels. Detailed mechanistic studies confirmed Cl^-/NO_3^- antiport mode as the primary mode of ion transport.

The dynamically gated ion transport process was achieved using two different sets of electromagnetic radiation at 365 nm and 450 nm, respectively, across HPTS-based lipid vesicles. Theoretical studies provided further insights into the self-assembly behaviour of channel forming molecules inside the lipid bilayer membrane and chloride transport through the channel lumen.

Author contributions

P. T. conceived the project and directed the experimental studies. M. A. performed the ion transport studies and photo-irradiation studies. S. S. and J. M. performed the theoretical studies. R. B. performed the synthesis and characterization of the compounds. A. M. performed the ion channel conductance studies. D. M. performed the morphological studies.

Data availability

Data for this paper, including synthesis, compound characterization, experimental procedures, and theoretical calculations, are available in the ESI.†

Conflicts of interest

There are no conflicts to declare.

Acknowledgements

References

1 H. Li, H. Valkenier, L. W. Judd, P. R. Brotherhood, S. Hussain, J. A. Cooper, O. Jurček, H. A. Sparkes, D. N. Sheppard and A. P. Davis, *Nat. Chem.*, 2016, **8**, 24–32.

2 K. A. Muraglia, R. S. Chorghade, B. R. Kim, X. X. Tang, V. S. Shah, A. S. Grillo, P. N. Daniels, A. G. Cioffi, P. H. Karp, L. Zhu, M. J. Welsh and M. D. Burke, *Nature*, 2019, **567**, 405–408.

3 S.-K. Ko, S. K. Kim, A. Share, V. M. Lynch, J. Park, W. Namkung, W. Van Rossom, N. Busschaert, P. A. Gale, J. L. Sessler and I. Shin, *Nat. Chem.*, 2014, **6**, 885.

4 T. Saha, M. S. Hossain, D. Saha, M. Lahiri and P. Talukdar, *J. Am. Chem. Soc.*, 2016, **138**, 7558–7567.

5 T. Saha, A. Gautam, A. Mukherjee, M. Lahiri and P. Talukdar, *J. Am. Chem. Soc.*, 2016, **138**, 16443–16451.

6 S.-P. Zheng, L.-B. Huang, Z. Sun and M. Barboiu, *Angew. Chem., Int. Ed.*, 2021, **60**, 566–597.

7 N. Sakai, K. C. Brennan, L. A. Weiss and S. Matile, *J. Am. Chem. Soc.*, 1997, **119**, 8726–8727.

8 S. J. Moore, C. J. E. Haynes, J. González, J. L. Sutton, S. J. Brooks, M. E. Light, J. Herniman, G. J. Langley, V. Soto-Cerrato, R. Pérez-Tomás, I. Marques, P. J. Costa, V. Félix and P. A. Gale, *Chem. Sci.*, 2013, **4**, 103–117.

9 N. Busschaert, M. Wenzel, M. E. Light, P. Iglesias-Hernández, R. Pérez-Tomás and P. A. Gale, *J. Am. Chem. Soc.*, 2011, **133**, 14136–14148.

10 L. Lien, D. C. J. Jaikaran, Z. Zhang and G. A. Woolley, *J. Am. Chem. Soc.*, 1996, **118**, 12222–12223.

11 Y. R. Choi, B. Lee, J. Park, W. Namkung and K.-S. Jeong, *J. Am. Chem. Soc.*, 2016, **138**, 15319–15322.

12 E. N. W. Howe, N. Busschaert, X. Wu, S. N. Berry, J. Ho, M. E. Light, D. D. Czech, H. A. Klein, J. A. Kitchen and P. A. Gale, *J. Am. Chem. Soc.*, 2016, **138**, 8301–8308.

13 Y. Kobuke, K. Ueda and M. Sokabe, *Chem. Lett.*, 2006, **24**, 435–436.

14 M. M. Tedesco, B. Ghebremariam, N. Sakai and S. Matile, *Angew. Chem., Int. Ed.*, 1999, **38**, 540–543.

15 M. R. Banghart, M. Volgraf and D. Trauner, *Biochemistry*, 2006, **45**, 15129–15141.

16 M. Ahmad, S. Metya, A. Das and P. Talukdar, *Chem. – Eur. J.*, 2020, **26**, 8703–8708.

17 M. Ahmad, D. Mondal, N. J. Roy, T. Vijayakanth and P. Talukdar, *ChemPhotoChem*, 2022, e202200002.

18 M. Ahmad, S. Chattopadhayay, D. Mondal, T. Vijayakanth and P. Talukdar, *Org. Lett.*, 2021, **23**, 7319–7324.

19 A. Kerckhoffs and M. J. Langton, *Chem. Sci.*, 2020, **11**, 6325–6331.

20 T. G. Johnson, A. Sadeghi-Kelishadi and M. J. Langton, *J. Am. Chem. Soc.*, 2022, **144**, 10455–10461.

21 Y. R. Choi, G. C. Kim, H.-G. Jeon, J. Park, W. Namkung and K.-S. Jeong, *Chem. Commun.*, 2014, **50**, 15305–15308.

22 W.-Z. Wang, L.-B. Huang, S.-P. Zheng, E. Moulin, O. Gavat, M. Barboiu and N. Giuseppone, *J. Am. Chem. Soc.*, 2021, **143**, 15653–15660.

23 C. Bao, M. Ma, F. Meng, Q. Lin and L. Zhu, *New J. Chem.*, 2015, **39**, 6297–6302.

24 M. Ahmad, N. J. Roy, A. Singh, D. Mondal, A. Mondal, T. Vijayakanth, M. Lahiri and P. Talukdar, *Chem. Sci.*, 2023, **14**, 8897–8904.

25 H. Fliegl, A. Köhn, C. Hättig and R. Ahlrichs, *J. Am. Chem. Soc.*, 2003, **125**, 9821–9827.

26 J. A. Malla, M. Ahmad and P. Talukdar, *Chem. Rec.*, 2022, **22**, e202100225.

27 R.-Y. Yang, C. Bao, Q.-N. Lin and L.-Y. Zhu, *Chin. Chem. Lett.*, 2015, **26**, 851–856.

28 Y. Zhou, Y. Chen, P.-P. Zhu, W. Si, J.-L. Hou and Y. Liu, *Chem. Commun.*, 2017, **53**, 3681–3684.

29 T. Liu, C. Bao, H. Wang, Y. Lin, H. Jia and L. Zhu, *Chem. Commun.*, 2013, **49**, 10311–10313.

30 R. Sharma, A. Vijay, S. Chattopadhayay, A. Mukherjee and P. Talukdar, *Chem. Commun.*, 2023, **59**, 3602–3605.

31 A. Roy, T. Saha, M. L. Gening, D. V. Titov, A. G. Gerbst, Y. E. Tsvetkov, N. E. Nifantiev and P. Talukdar, *Chem. – Eur. J.*, 2015, **21**, 17445–17452.

32 B. L. Schottel, H. T. Chifotides and K. R. Dunbar, *Chem. Soc. Rev.*, 2002, **37**, 68–83.

33 D. Mondal, A. Sathyan, S. V. Shinde, K. K. Mishra and P. Talukdar, *Org. Biomol. Chem.*, 2018, **16**, 8690–8694.

34 T. M Fyles, R Knoy, K Müllen and M Sieffert, *Langmuir*, 2001, **17**, 6669–6674.

35 T. Saha, A. Gautam, A. Mukherjee, M. Lahiri and P. Talukdar, *J. Am. Chem. Soc.*, 2016, **138**, 16443–16451.

36 O. S. Smart, J. Breed, G. R. Smith and M. S. Sansom, *Biophys. J.*, 1997, **72**, 1109–1126.